ACS OMEGA

http://pubs.acs.org/journal/acsodf

Article

Harnessing ROS-Induced Oxidative Stress for Halting Colorectal Cancer *via* Thiazolidinedione-Based SOD Inhibitors

Mohamed Nabil Abd Al Moaty, El Sayed H. El Ashry, Laila Fathy Awad,* Asmaa Mostafa, Marwa M. Abu-Serie, and Mohamed Teleb

Cite This: *ACS Omega* 2022, 7, 21267−21279

Read Online

ACCESS | Metrics & More | Article Recommendations | Supporting Information

ABSTRACT: Based on the "canonical" view of reactive oxygen species' (ROS) contribution to carcinogenesis, ROS induce oxidative stress and promote various tumor progression events. However, tumor cells also need to defend themselves against oxidative damage. This "heresy" was supported by several recent studies underlining the role of cellular antioxidant capacity in promoting metastasis and resistance to chemotherapy. Accordingly, harnessing the ROS-induced oxidative stress via selective suppression of the cancer antioxidant defense machinery has been launched as an innovative anticancer strategy. Within this approach, pharmacological inhibition of superoxide dismutases (SODs), the first-line defense antioxidant enzymes for cancer cells, selectively kills tumor cells and circumvents their acquired resistance. Various SOD inhibitors have been introduced, of which some were tolerated in clinical trials. However, the hit SOD inhibitors belong to diverse chemical classes and lack comprehensive structure−activity relationships (SAR). Herein, we probe the potential of newly synthesized benzylidene thiazolidinedione derivatives to inhibit SOD in colorectal cancer with special emphasis on their effects on correlated antioxidant enzymes aldehyde dehydrogenase 1 (ALDH1) and glutathione peroxidase (GPx). This may possibly bring a new dawn for utilizing thiazolidinediones (TZDs) in cancer therapy through SOD inhibition mechanisms. The preliminary 3-(4,5-dimethylthiazol-2-yl)-2,5-diphenyltetrazolium bromide (MTT) assay showed that all of the evaluated TZDs exhibited excellent safety profiles on normal human cells, recording an EC100 of up to 47.5-folds higher than that of doxorubicin. Compounds **3c**, **6a**, and **6e** (IC50 = 4.4−4.7 μM) were superior to doxorubicin and other derivatives against Caco-2 colorectal cancer cells within their safe doses. The hit anticancer agents inhibited SOD (IC50 = 97.2−228.8 μM). Then, they were selected for further in-depth evaluation on the cellular level. The anticancer IC50 doses of **3c**, **6a**, and **6e** diminished the antioxidant activities of SOD (by 29.7, 70.1, and 33.3%, respectively), ALDH1A (by 85.92, 95.84, and 86.48%, respectively), and GPX (by 50.17, 87.03, and 53.28%, respectively) in the treated Caco-2 cells, elevating the Caco-2 cellular content of ROS by 21.42, 7.863, and 8.986-folds, respectively. Docking simulations were conducted to display their possible binding modes and essential structural features. Also, their physicochemical parameters and pharmacokinetic profiles formulating drug-likeness were computed.

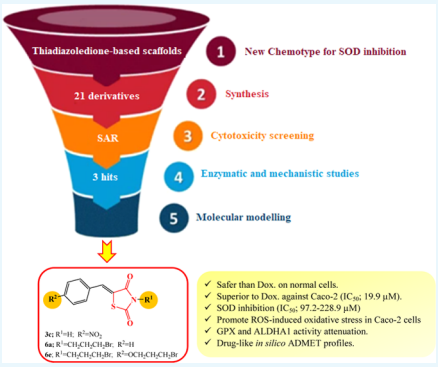

1. INTRODUCTION

Dysregulation of the cell energetics is a well-known hallmark of carcinogenesis.[1] Tumor cells produce more reactive oxygen species (ROS),[2] causing oxidative stress and promoting tumor progression.[3] Hence, various anticancer agents were introduced to halt oxidative stress *via* scavenging ROS, defending against their destructive action or even inhibiting their production.[4−8] While various antioxidants appear to be chemopreventive agents, the clinical outcomes of antioxidant-based cancer therapy are nonconclusive, if not disappointing. This could be attributed to the fact that ROS also mediate natural defense mechanisms against tumor propagation. Recently, harnessing oxidative stress *via* selective suppression of the cancer antioxidant defense mechanisms has been adopted as an innovative strategy for cancer therapy.[9] In this regard, the mitochondrial antioxidant enzymes superoxide dismutases (SODs) have received growing attention as survival factors for cancer cells.[10] SODs are ubiquitous components of the normal cellular antioxidant system. As firstly reported by McCord and Fridovich, SODs protect the cellular machinery from free radical-induced damage by catalyzing superoxide ions' disproportionation to oxygen and hydrogen peroxide,[11] which is then detoxified to water and oxygen *via* glutathione peroxidase (GPx).[12] Several families of SODs have been identified. The catalytic activity of each family relies upon specific redox-active metal ions, which are manganese, iron, copper, zinc, or nickel ions. The accentuations of their normal

Received: April 18, 2022
Accepted: May 26, 2022
Published: June 7, 2022

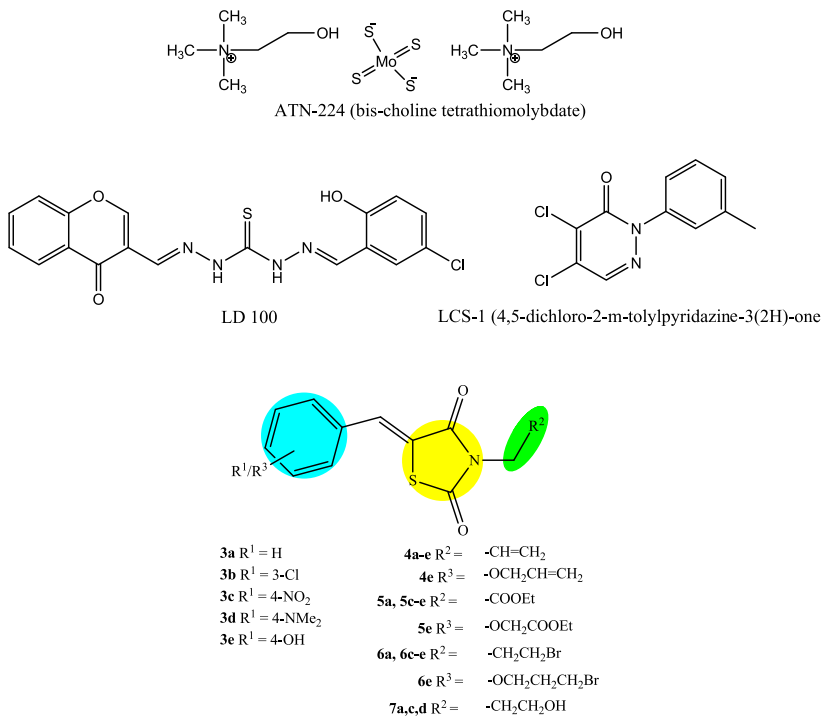

Figure 1. Reported SOD inhibitors and target thiazolidinedione.

functions are associated to several diseases and malignancies.[13] The strongest connection between SODs and abnormalities is found for the copper and zinc-dependent forms.[14]

Despite the fact that SODs can supress tumor incidence, several lines of evidence have disclosed the unexpected oncogenic potential of SODs. It is clear that SOD is crucial for cancer cell resistance to cytotoxic agents and prevention of the oncogene-induced apoptosis triggered by p53, as evidenced by its elevated levels in different stages of various neoplasms, in a fashion that correlates with the malignancy degree.[15−19] SODs enhance metastasis and the invasiveness of cancers *via* promoting epithelial−mesenchymal transition of pancreatic cancer cells prior to activation of the H_2O_2/ERK/NF-κB axis.[20] Interestingly, halting angiogenesis by disulfiram, a potential Cu/Zn SOD inhibitor, also raises the possibility that attenuation of SOD activity may be adopted in the treatment of angiogenesis-dependent pathologies.[21,22] Furthermore, SOD suppression was found to be a promising strategy to reduce the stemness and tumorigenicity of breast cancer cells expressing aldehyde dehydrogenase 1-positive (ALDH1+).[23] This finding highlights a possible correlation between SOD and ALDH that catalyzes reactive aldehyde oxidation to maintain cellular homeostasis. However, overexpression of ALDH isozymes has been reported in various cancers and associated with relapses; thus, various inhibitors of ALDH enzymes have been developed as potential anticancer agents.[24]

Review of the literature revealed various anticancer SOD inhibitors of diverse chemical classes, such as dithiocarbamate derivatives (e.g., diethylthiocarbamate salts and disulfiram) and the bis-choline tetrathiomolybdate ATN-224, an orally bioavailable inhibitor of SOD (IC_{50} = 330 nM), *via* copper chelation, which attenuates angiogenesis and tumor proliferation. Interestingly, ATN-224 was well tolerated in phase I and II anticancer clinical trials.[25,26] Further investment in tailoring efficient copper chelators can lead to the introduction of LD100, a potent SOD inhibitor.[27]

4,5-Dichloro-2-(3-tolyl)pyridazin-3(2*H*)-one (LCS-1) is another SOD inhibitor discovered from high-throughput screening of promising anticancer agents that preferentially inhibits lung adenocarcinoma cell growth.[28,29] LCS-1 binds to and inhibits SOD *in vitro*. Mechanistic studies have revealed that the sensitivity of tumor cells to LCS-1 is closely related to SOD expression level.[29] Motivated by such approach, the current study portrays the design, synthesis, and evaluation of new SOD inhibitors as potential anticancer agents for colorectal cancer given the association between SOD levels and colorectal cancer staging and grade of differentiation.[15]

2. DESIGN RATIONALE

As illustrated (Figure 1), the reported SOD inhibitors belong to diverse chemical classes with limited structure−activity relationship (SAR) data. The introduction of new inhibitors with privileged scaffold will pave the way for further studies towards establishing comprehensive SAR against SOD. Herein, thiazolidinedione (TZD), the widely represented pharmacophore,[30−32] was elected as a new core for introducing SOD inhibitors. The adopted design strategy relied on probing the potential of TZD to inhibit Cu/Zn SOD, inspired by its intrinsic property to coordinate the active site Zn of various metalloenzymes such as histone deacetylase 4,[33] and carbonic anhydrases.[34] In this regard, a series of 5-arylidene-2,4-thiazolidinediones were synthesized and derivatized to introduce various functionalities for enriching the SAR.

All of the synthesized derivatives (Scheme 1) were initially screened for their cytotoxic effect on normal fibroblasts to assess their safety profiles, followed by evaluating their anticancer activities against human colon cancer (Caco-2) cells *via* 3-(4,5-dimethylthiazol-2-yl)-2,5-diphenyltetrazolium bromide (MTT) assay as previously reported.[35−37] The most promising derivatives were subjected to SOD inhibition assay.

https://doi.org/10.1021/acsomega.2c02410
ACS Omega 2022, 7, 21267−21279

Scheme 1. Synthesis of *N*-Alkyl-5-arylidene-2,4-thiazolidinedione 4−7[a]

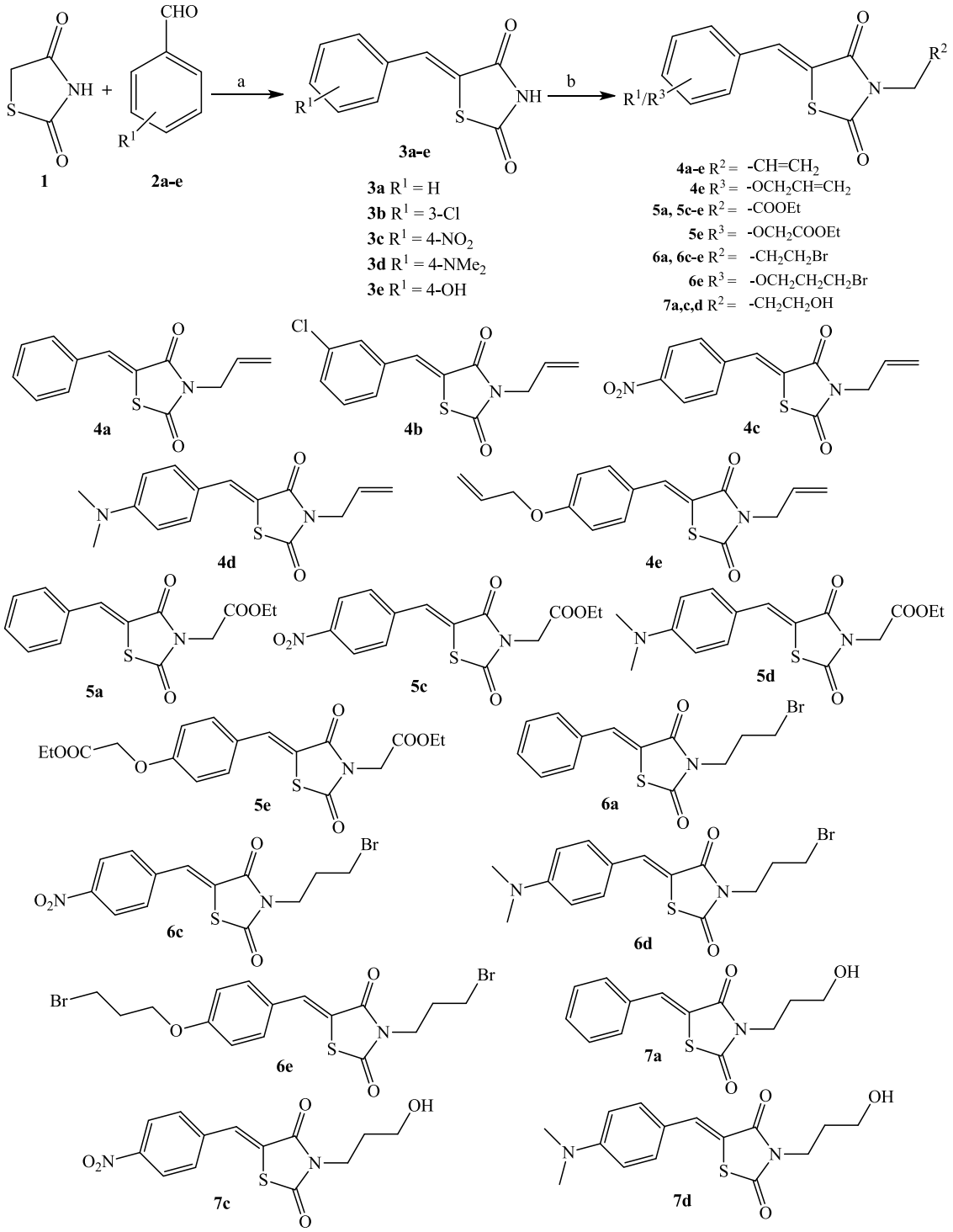

[a]Reagents and conditions: (a) anhydrous sodium acetate, EtOH, reflux 3−15 h; (b) alkyl halide, anhydrous K_2CO_3, dimethylformamide (DMF), ultrasound irradiation for 20−60 min at room temperature.

The study was extended to explore the inhibitory activities of the hit TZDs against the correlated antioxidant enzymes ALDH1 and GPX in Caco-2 cells; then, cellular ROS was quantified after treatment of Caco-2 cells with the studied derivatives. Docking simulations were conducted to predict their binding modes and pharmacophoric features contributing to interactions with the receptor sites. Finally, their physicochemical parameters and pharmacokinetic profiles were computed.

3. RESULTS AND DISCUSSION

3.1. Chemistry. Synthesis of 2,4-thiazoldinedione (TZD) was attempted by the reaction of chloroacetic acid and thiourea in the presence of HCl under reflux for 10−12 h. Structure modification of the TZD core has been carried out

https://doi.org/10.1021/acsomega.2c02410
ACS Omega 2022, 7, 21267−21279

using substitution at both the NH and/or the methylene groups. 5-Arylidene-2,4-thiazolidinediones have been synthesized through Knoevenagel condensation of aromatic aldehydes with TZD using various catalysts.[38] Thus, reaction of 2,4-thiazolidinedione **1** with aromatic aldehydes **2a−e** in the presence of anhydrous sodium acetate under reflux for 3−15 h afforded the respective 5-arylidene derivatives **3a−e** in 56−86% yield. Use of ultrasound irradiation in organic synthesis has become a more efficient, safe, convenient, and simple method. Ultrasound irradiation reactions are much more advantageous than traditional thermal methods in terms of reaction rates, yield, purity of the products, and selectivity.[39−41] Thus, alkylation of the 5-arylidene-2,4-thiazolidinedione **3a−e** with different alkyl halides was established under ultrasound irradiation in DMF in the presence of anhydrous potassium carbonate at room temperature in order to afford the respective *N*-alkyl-5-arylidene-2,4-thiazolidinedione analogues **4−7** with good yield within 20−60 min (Scheme 1).

Accordingly, treatment of 5-arylidene-2,4-thiazolidinediones **3a−e** with allyl bromide in DMF in the presence of potassium carbonate under ultrasound irradiation for 25−30 min at room temperature afforded the respective *N*-allyl derivatives **4a−e** in 52−64% yield. The structures of compounds **4a−d** were elucidated from their spectral data. The ^{1}H NMR spectra showed the disappearance of a characteristic signal corresponding to the N−H proton in the downfield region and instead, the allyl proton signals were assigned. The N-CH_2 protons were assigned as a doublet at δ_H 4.37−4.40 ppm, whereas the multiplet peak resonated at δ_H 5.83−5.93 ppm was corresponding to the C<u>H</u>=CH_2 proton. The terminal CH=<u>CH_2</u> protons were assigned as two doublets at δ_H 5.23−5.36 ppm with J_{gem} 12.0−16.0 Hz. The benzylidene proton was assigned as a singlet peak at δ_H 7.85−7.94 ppm. In addition, the characteristic carbon signals of the allyl moiety were assigned at δ_C 130.6−134.7, 118.5−119.5, and 43.7−44.2 ppm, corresponding to <u>CH_2</u>=CH, CH_2=<u>C</u>H, and N-CH_2, respectively, whereas the benzylidene carbon was assigned at δ_C 134.0−149.0 ppm. The carbonyl groups of the thiazolidinedione ring were assigned at the downfield region at δ_C 166.3−168.1 ppm, while C-4 was resonated at δ_C 112.5−126.0 ppm. On the other hand, the reaction of allyl bromide with 5-(4-hydroxybenzylidene)-2,4-thiazolidinedione **3e** under the same reaction conditions gave the *O*-,*N*-diallyl derivative **4e**. The structure of **4e** was confirmed from the absence of both the NH of the thiazolidine ring and the phenolic OH protons in the ^{1}H NMR spectrum, and instead, two allyl groups were present. The two doublets corresponding to the NCH_2 and OCH_2 protons were assigned at δ_H 4.37 and 4.63 ppm, respectively, whereas their respective carbons were resonated at δ_C 43.78 and 68.96 ppm, respectively. Moreover, the <u>CH_2</u>=CHCH_2N and <u>CH_2</u>=CHCH_2O protons were assigned as three doublet of doublets at δ_H 5.25−5.48 ppm with J < 1 Hz, 4 Hz and J_{gem} = 12 Hz; these protons were correlated to the carbons assigned at δ_C 118.3 and 118.8, respectively. The CH_2=C<u>H</u>CH_2N and CH_2=C<u>H</u>CH_2O protons were resonated as multiplet signals at δ_H 5.83−5.93 and 6.03−6.12 ppm, respectively, correlated to the carbon signals assigned at δ_C 130.3 and 132.4 ppm, respectively.

Moreover, the reaction of the 5-arylidene derivatives **3a, 3c**, and **3d** with ethyl bromoacetate in DMF and in the presence of anhydrous potassium carbonate under the influence of ultrasound irradiation for 30−60 min at room temperature afforded the ethyl *N*-acetate derivatives **5a, 5c**, and **5d**, respectively, whereas the 4-hydroxybenzylidene derivatives **3e** afforded the respective *O*-,*N*-derivative **5e** as a result of the double alkylation on both the NH and OH groups; this agreed with Ionut et al.[42] and Marc et al.,[43] who reported the synthesis of the *O*-,*N*-dialkylated derivative under microwave irradiation and conventional heating. However, Nawale et al.[44] reported that only the phenolic OH was alkylated with ethyl chloroacetate in acetone under reflux.

The characteristic signals indicating the alkylation with the ethylacetate group were assigned from the ^{1}H and ^{13}C NMR spectra of the synthesized compounds **5a** and **5c-e**. Thus, the NCH_2 protons were resonated as a singlet at δ_H 4.43−4.50 ppm, which correlated with its carbon assigned at δ_C 37.3−42.1 ppm. The ethyl protons were assigned as a triplet ($C\underline{H}_3CH_2$-) and a quartet ($CH_3C\underline{H}_2$-) peak at δ_H 1.24−1.32 ppm and δ_H 4.20−4.27 ppm, respectively, whereas their carbons were assigned at δ_C 14.1 and 62.0−62.4 ppm, respectively. On the other hand, the NMR of compound **5e** showed the presence of a quartet pattern at δ_H 1.30−1.35 ppm as a result of the overlap of the two triplets that were assumed for the methyl protons. Alternatively, the <u>CH_2</u>CH_3 protons were also overlapped and resonated as two quartet patterns at δ_H 4.24−4.34 ppm. Other protons and carbons are detailed and reported in the experimental section.

Alternatively, the reaction of **3a, 3c**, and **3d** with 1,3-dibromopropane in the presence of anhydrous potassium carbonate in DMF for 20−40 min afforded the *N*-(3-bromopropyl)-2,4-thiazolidinone derivatives **6a, 6c**, and **6d**, respectively, as verified from the spectral data of these compounds. Their ^{1}H NMR spectra showed three characteristic signals for the propyl moiety that resonated as two triplets and a quintet at δ_H 3.92−3.96, 3.43−3.44, and 2.27−2.29 ppm corresponding to NCH_2, CH_2Br, and $NCH_2C\underline{H}_2CH_2$Br, respectively. The *N*-(3-bromopropyl) derivatives **6a**, **6c**, and **6d** were further confirmed from the assignment of a singlet integrating proton at δ_H 7.86−7.95 ppm corresponding to the arylidene C<u>H</u>=C proton. Moreover, their ^{13}C NMR spectra showed two carbonyl signals at δ_C 167.9−165.9 and one carbon signal corresponding to the benzylidene carbon <u>C</u>H=C resonated at δ_C 134.0−152.0 ppm.

On the other hand, the reaction of 5-(4-hydroxybenzylidene)-2,4-thiazoldinedione **3e** with 1,3-dibromopropane afforded the *O*-,*N*-dialkylated derivative **6e**, as confirmed from the NMR spectra. The ^{1}H NMR spectra of **6e** showed two quintets, each of them integrating two protons at δ_H 2.37 and 2.27 ppm corresponding to $OCH_2C\underline{H}_2CH_2$Br and $NCH_2C\underline{H}_2CH_2$Br, whereas the OCH_2 and NCH_2 protons were resonated as two triplets at δ_H 4.20 and 3.92 ppm, respectively. The CH_2Br protons were resonated at a lower frequency as two triplets at δ_H 3.43 and 3.63 ppm. Alternatively, the ^{13}C NMR spectrum of **6e** showed the presence of six signals corresponding to the propyl carbon moieties, which were assigned at δ_C 29.5, 29.7 ppm (2 $CH_2C\underline{H}_2CH_2$Br), 30.8, 32.1 (2 CH_2Br), 40.6 (NCH_2), and 65.5 ppm (OCH_2). Moreover, only two carbonyl signals corresponding to the thiazolidine-2,4-dione moiety were resonated at δ_C 166.4 and 168.1 ppm.

Alternatively, the reaction of **3a, 3c**, and **3d** with 3-chloropropanol under ultrasound irradiation for 25−45 min at room temperature in DMF and in the presence of anhydrous potassium carbonate afforded the respective 3-(3-hydroxypropyl)-5-(arylidene)-2,4-thiazolidinediones **7a, 7c**, and **7d**, respectively. The characteristic signals for the 3-hydroxypropyl

https://doi.org/10.1021/acsomega.2c02410
ACS Omega 2022, 7, 21267−21279

moiety were elucidated from their ^{1}H and ^{13}C NMR spectra. Thus, the NCH_2 protons were assigned as a triplet at δ_H 3.96 ppm and correlated to the carbon signal at δ_C 38.5 for compound **7a** (measured in $CDCl_3$). However, the NCH_2 signals for **7c** and **7d** (measured in DMSO-d_6) were masked under the solvent peak. The $C\underline{H_2}OH$ protons for compound **7a** were assigned as a triplet at δ_H 3.65, whereas those for compounds **7c** and **7d** were assigned as a quartet at δ_H 3.47 and 3.45 ppm, respectively, and were correlated with their carbon signals at δ_C 58.9 ppm. The quintet corresponding to $NCH_2C\underline{H_2}CH_2OH$ was assigned at δ_H 1.92, 1.75, and 1.72 ppm for **7a**, **7c**, and **7d**, respectively, whereas its carbon was resonated at δ_C 30.6−30.9 ppm. The hydroxyl proton was resonated as an exchangeable broad singlet at δ_H 2.15 for **7a**, while for **7c** and **7d** it resonated as a triplet at 4.61 and 4.58 ppm, respectively.

3.2. Biological Evaluation. *3.2.1. Cytotoxicity Screening on Normal Human Cells.* Firstly, the newly synthesized thiazolidine-2,4-dione derivatives were screened *via* MTT assay for their cytotoxic activities against normal human cells (Wi-38) to assess their safety profiles. Thus, the safe concentration (EC_{100}), at which 100% of normal cell viability is attained, was calculated using the percentage of cell viability at serial concentrations of the studied derivatives, and compared to the reference chemotherapeutic drug (Table 1).

Table 1. Cytotoxicity of the Thiazolidine-2,4-dione Derivatives 4−7 on Normal Human Cells (Wi-38), Expressed as EC_{100} (μM)

compound	EC_{100} (μM)[a]
1	22.047 ± 0.434
3a	19.679 ± 3.105
3b	5.621 ± 0.071
3c	6.0653 ± 0.127
3d	25.345 ± 0.655
3e	6.727 ± 0.040
4a	58.916 ± 10.698
4b	9.902 ± 2.360
4c	7.078 ± 0.136
4d	28.971 ± 2.121
4e	30.971 ± 0.971
5a	30.456 ± 0.456
5c	8.573 ± 0.409
5d	16.179±6.066
5e	8.417 ± 0.004
6a	18.938 ± 0.975
6c	13.424 ± 1.130
6d	14.776 ± 1.125
6e	10.683 ± 2.384
7a	18.923 ± 1.959
7c	11.439 ± 0.927
7d	12.073 ± 3.577
DOX	1.239 ± 0.285

[a]All values are expressed as mean ± standard error of mean (SEM).

Based on the high EC_{100} indicating a high safety on cells, the results revealed notable promising safety profiles of the synthesized series, where all compounds were safer than the reference chemotherapy doxorubicin (DOX). Compound **4a** came at the top of the series with the highest detected EC_{100} (58.92 μM) being approximately 47.5-folds safer than DOX, followed by **5a**, **4e**, and **4d** (EC_{100} 30.97−28.97 μM). **3d** (EC_{100} 25.35 μM) and **1** (EC_{100} 22.05 μM) were of relatively moderate safety. Other derivatives exhibited lower EC_{100} values ranging from 19.68 to 5.62 μM.

3.2.2. Anticolorectal Cancer Activity. The studied compounds were subjected to anticancer evaluation *via* MTT assay against human colon cancer Caco-2 cells and compared to DOX as reference chemotherapy (Table 2). To accurately assess the growth inhibitory potential of these compounds, the half-maximal inhibitory concentration (IC_{50}), at which Caco-2 growth rate is inhibited by 50% relative to the untreated cells, was estimated. The low value of this dose was used as an indicator of high anticancer potential. All derivatives were superior to the reference (IC_{50}; 19.89 μM) against Caco-2, except **3a**, within their safe doses (EC_{100}). Compounds **6e** (IC_{50}; 4.41 μM), **3c** (IC_{50}; 4.71 μM), and **6a** (IC_{50}; 4.73 μM) exhibited the highest anticancer potentials among the evaluated derivatives. These compounds (**3c**, **6a**, and **6e**) caused severe shrinkage and collapse of Caco-2 cells, as shown in Figure 2. The remainder compounds were relatively moderate, recording IC_{50} ranging from 6.51 to 13.75 μM. Accordingly, they (**3c**, **6a**, and **6e**) were selected as our hit thiazolidine-2,4-dione derivatives for further mechanistic studies.

Table 2. Cytotoxicity of the Thiazolidine-2,4-Dione Derivatives 4−7 on Human Colon Cancer (Caco-2), Expressed as IC_{50} (μM)

compound	IC_{50} (μM)[a]
1	12.054 ± 3.253
3a	74.627 ± 8.310
3b	7.028 ± 0.315
3c	**4.718 ± 0.602**
3d	8.954 ± 0.631
3e	8.478 ± 0.599
4a	11.989 ± 1.358
4b	13.755 ± 0.789
4c	6.517 ± 0.077
4d	7.062 ± 0.005
4e	12.204 ± 3.124
5a	8.201 ± 0.135
5c	6.668 ± 0.118
5d	8.241 ± 2.589
5e	8.571 ± 0.942
6a	**4.739 ± 0.021**
6c	10.407 ± 0.499
6d	7.940 ± 0.599
6e	**4.413 ± 0.546**
7a	10.152 ± 0.770
7c	6.765 ± 0.096
7d	7.118 ± 0.010
DOX	19.894 ± 2.370

[a]All values are expressed as mean ± standard error of mean (SEM).

3.2.3. SOD Inhibition. SOD inhibition profiles of the selected anticancer hits **3c**, **6a**, and **6e** were detected and compared to the reference sodium diethyldithiocarbamate (DDC) using the superoxide dismutase kit from R&D Systems according to the manufacturer's instructions. In the assay, superoxide anions generated by xanthine oxidase (XOD) convert nitrobluetetrazolium (NBT) to NBT-diformazan, which absorbs light at λ = 550 nm. SOD reduces the superoxide anion concentration and thereby lowers the rate of

https://doi.org/10.1021/acsomega.2c02410
ACS Omega 2022, 7, 21267−21279

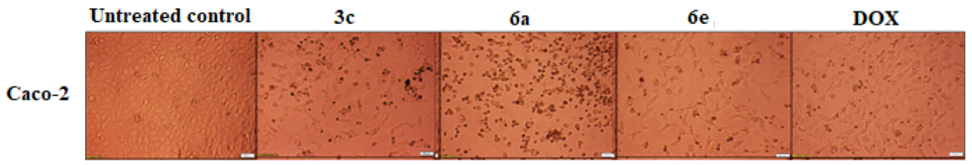

Figure 2. Morphological changes of Caco-2 cells after 72 h treatment with **3c, 6a**, and **6e** compared to doxorubicin (DOX).

NBT-diformazan formation. SOD activity was determined based on the difference between the control and test. The results (Table 3) showed that 5-(4-(3-bromopropoxy)-benzylidene)-3-(3-bromopropyl)thiazolidine-2,4-dione **6e** was the most potent among the groups, followed by the 5-benzylidene derivative **6a** and 5-(4-nitrobenzylidene)-thiazolidine-2,4-dione **3c**, respectively.

Table 3. SOD Inhibitory Activities of the Selected Thiazolidine-2,4-diones 3c, 6a, and 6e[a]

compound no.	IC_{50} (μM)
3c	228.87 ± 6.75
6a	154.42 ± 5.92
6e	97.24 ± 3.84
DDC	23.04 ± 1.62

[a]All values are expressed as mean ± SEM.

3.2.4. Inhibition of the Antioxidant Enzymes in Colorectal Cancer Cells (Caco-2). The most promising TZDs **3c, 6a**, and **6e** were selected for further in-depth evaluation, wherein mechanistic studies were conducted to study their potential to inhibit the antioxidant activities on a cellular level compared to the chemotherapeutic agent DOX owing to its prooxidant activities. The results showed that the IC_{50} doses of these TZDs diminished the intracellular SOD by 70.14, 29.74, and 33.35%, respectively, compared to 30.78% for DOX (Figure 3A) in the treated Caco-2 cells. The compounds were also tested for their inhibitory activities against ALDH1A and GPX being directly correlated to the cellular ROS content. Interestingly, compounds **3c, 6a**, and **6e** inhibited Caco-2 ALDH1A activity by 85.92, 95.84, and 86.48%, respectively (Figure 3B). Meanwhile, DOX revealed the lowest ALDH1A inhibition potency of about 4.800%. Regarding the activity of glutathione peroxidase (GPx), these compounds and DOX suppressed it by 50.17, 87.03, 53.28, and 40.31% in Caco-2 cells after 72 h of incubation, respectively, as demonstrated in Figure 3C.

3.2.5. Determination of Cellular ROS in Colorectal Cancer (Caco-2). In light of the aforementioned results, the cellular ROS in Caco-2 was determined after treatment with the studied derivatives **3c, 6a**, and **6e** by utilizing their anticolorectal cancer IC_{50} (Table 2). The results (Figure 4) revealed that the Caco-2 cellular content of ROS increased by 7.863, 21.42, and 8.986-folds in the treated Caco-2 cells relative to the untreated cells after incubation with the investigated compounds. Also, Figure 4 shows that the reference chemotherapeutic drug (DOX) had a lower ROS generation potency than the studied derivatives because DOX increased the cellular ROS level by only 4.065-folds compared to the untreated Caco-2 cells.

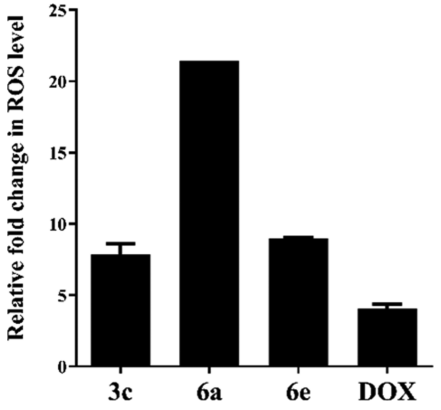

Figure 4. Fold increment in cellular ROS level in Caco-2 cells treated with **3c, 6a**, and **6e** as well as DOX relative to the untreated cells.

3.3. Molecular Modelling. *3.3.1. Docking of the Active TZDs **3c, 6a, and 6e** into SOD.* Docking simulations were performed by MOE 2015.10,[45] to predict the probable binding modes of the hit TZDs into the SOD active site and to possibly justify the rationalized design strategy. The crystal structure of SOD1 retrieved from the protein data bank (PDB ID: 6FOI)[46] was prepared by eliminating unwanted residues, ligands, and water molecules, and then subjected to the default "Structure

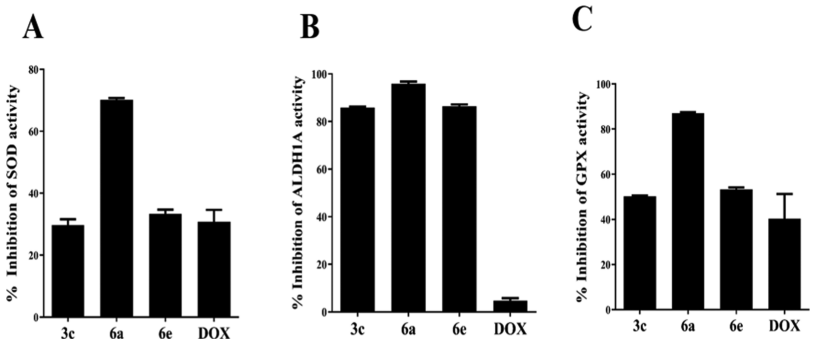

Figure 3. Inhibitory potency of the most effective anticancer compounds (**3c, 6a**, and **6e**) as well as DOX on the activities of antioxidant enzymes: (A) SOD, (B) ALDH1A, and (C) GPX after 72 h of incubation with Caco-2 cells.

https://doi.org/10.1021/acsomega.2c02410
ACS Omega 2022, 7, 21267−21279

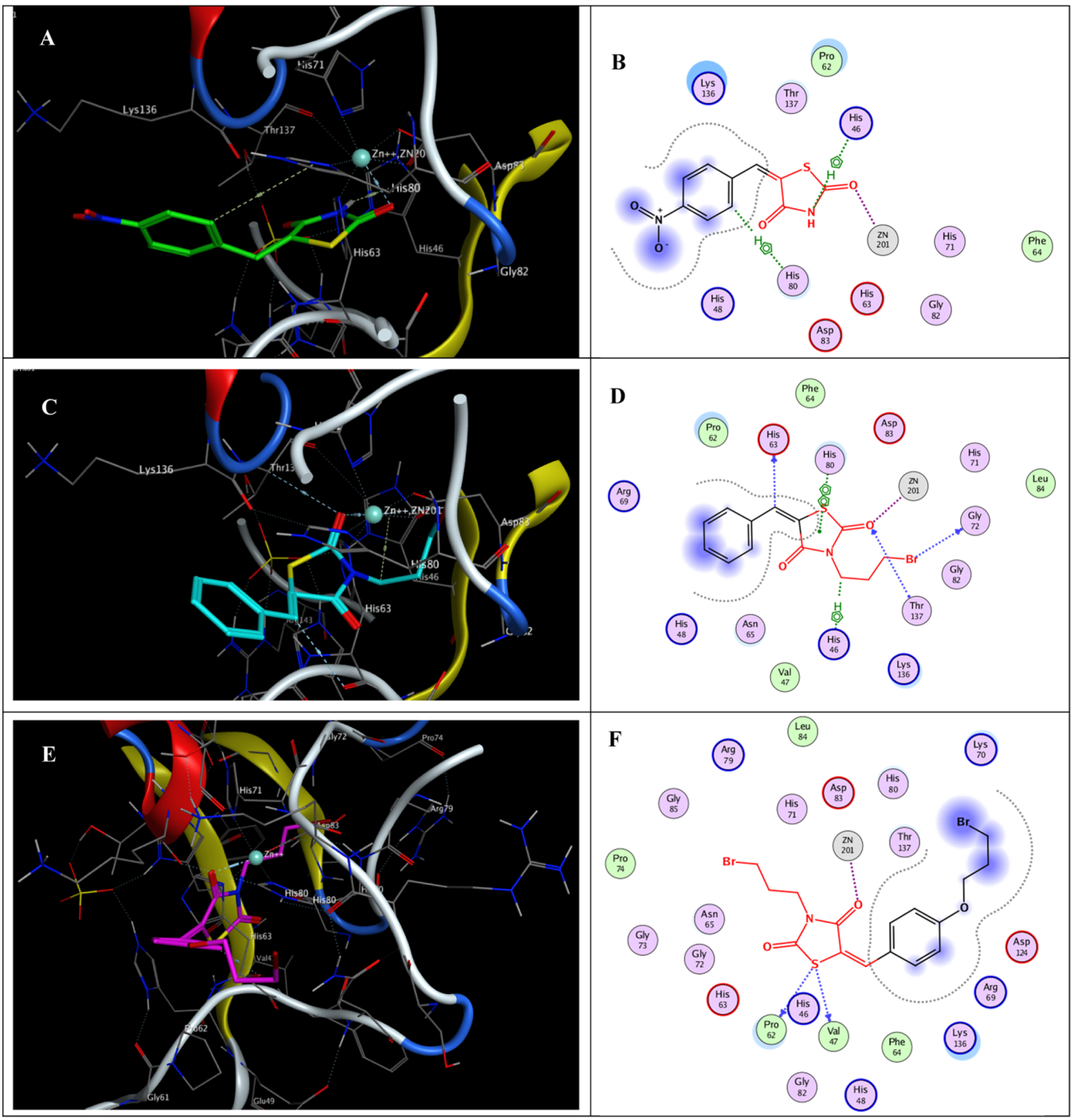

Figure 5. (A) 3D binding mode of **3c** (green sticks), (B) two-dimensional (2D) binding mode of **3c**, (C) 3D binding mode of **6a** (cyan sticks), (D) 2D binding mode of **6a**, (E) 3D binding mode of **6e** (cyan sticks), and (F) 2D binding mode of **6e** into SOD (PDB ID: 6FOI)[46] Zn domain.

preparation" module settings, where hydrogen atoms were added, hydrogen bonds were optimized, and atomic clashes were removed. The studied TZDs were built *in silico*, energy minimized, and optimized using the default MOE settings, then located in the active site, specifically in the vicinity of the enzyme Zn. The docking protocol was conducted by employing the Triangular matcher algorithm as the ligand placement method and α HB as the scoring function, generating the top 10 nonredundant poses of the conformers with the lowest binding energies. Among the top-ranked poses according to docking scores and molecular interactions (Figure 5), the TZD localization into SOD1 can be stabilized mainly *via* both coordination to the SOD Zn as well as hydrogen bonds and other interactions with key SOD1 residues, particularly those normally coordinating the enzyme Zn. Interestingly, the TZD core *C2* carbonyl oxygens of the hit TZDs **3c**, **6a**, and **6e** were predicted to coordinate Zn, supporting the design rationale. The nitrobenzylidene TZD **3c** (ΔG = −2.99 kcal/mol) displayed H−π interactions with His46 and His80, through the TZD core *NH* and the *p*-nitrophenyl ring. The relatively more active SOD inhibitor TZD derivative **6a** (ΔG = −1.11 kcal/mol) posed additional hydrogen bonding and π−π interactions linking the TZD core and enzymes Thr137 and His80, respectively. The *N*-

https://doi.org/10.1021/acsomega.2c02410
ACS Omega 2022, 7, 21267−21279

bromopropyl appendage displayed hydrogen bond with Gly72 and H−π bond with His46. Furthermore, hydrogen bond interaction between the benzylidene *CH* and the key residue His63 (normally coordinating Zn) was observed. Concerning the active SOD inhibitor **6e** (ΔG = −4.47 kcal/mol), the TZD core sulfur was able to interact with the SODs Val47 and Pro62 *via* hydrogen bonding interactions.

Taking all together, the illustrated binding modes of the investigated derivatives (Figure 5) were nearly correlated with their *in vitro* and cell-based SOD inhibitory profiles (Table 3), supporting the design rationale and highlighting the potential of TZDs as a privileged scaffold for introducing SOD inhibitors.

3.3.2. In Silico Physicochemical Properties, ADMET, and Drug-Likeness. Recently, the medicinal chemistry sector of drug discovery research adopts *in silico* ADMET prediction and computational drug-likeness studies as reliable tools for lead identification. Herein, various physicochemical properties formulating important ADME and drug-likeness parameters of the most promising 2,4-thiazolidinedione derivatives were computed by employing *SwissADME*[47] software (Table 4). Interestingly, the three studied compounds were in full accordance to Lipinski's,[48] Veber's,[49] Muegge's,[50] and Ghose's[51] bioavailability parameters. The compounds displayed predicted drug-like TPSA (<140−150 A^2), high intestinal absorption, and acceptable aqueous solubility. Notably, **3c** recorded excellent predicted aqueous solubility. They were also predicted to lack cytochrome P450 (CYP3A and CYP2D6) inhibition, except **6e** regarding CYP3A. All compounds displayed high predicted intestinal absorption. Both **6a** and **6e** were predicted to cross the blood−brain barrier, while **3c** was predicted to be devoid of any CNS side effects. PROTOX,[52] the toxicity predictor program, predicted the average lethal dose (LD_{50}) of the studied compounds in rodents and classified it according to the Globally Harmonized System of Classification and Labeling of Chemicals (GHS) as class IV concerning acute oral toxicity. Interestingly, the compounds were also devoid of any predicted hepatotoxicity. In light of the abovementioned data, the synthesized 2,4-thiazolidinedione derivatives could be considered druggable.

3.4. Structure−Activity Relationship. In light of the aforementioned assays, the structure−activity relationship of the synthesized derivatives can be deduced. The general cytotoxic activity pattern reflects promising anticancer potential, as displayed by the designed TZD scaffold. However, the anticancer profile of each derivative regarding safety and activity was a function of the terminal benzylidene and N3-substitution. The *N*3-ally-substituted benzylidene derivative **4a** exhibited the highest safety profile. Allyloxy **4e** or dimethylamino **4d** substitution on the benzylidene ring slightly affected the scaffold's safety. Similarly, *N*3-substitution with ethylacetate **5a** showed a slightly lower safety than the *N*3-ally-substituted analogue **4a**. Deletion of *N*3-substitution **3d** also lowered the derivative's safety. Other substitutions showed lower and comparable EC_{100} values. Obviously, the TZD derivatives bearing 4-nitrobenzylidene **3c**, *N*3-3-bromopropyl **6a**, or terminal 3-bromopropoxy together with substituting the TZD *N*3 with 3-bromopropyl **6e** conferred the highest anticancer activity towards Caco-2 cells. On the other hand, the unsubstituted benzylidenethiazolidine-2,4-dione derivative **3a** was relatively devoid of antiproliferative activity. However, diversifying the terminal benzylidene substitution restored considerable anticancer potency and controlled selectivity, as

Table 4. In Silico Prediction of Physicochemical Properties, ADMET, and Drug-Likeness of the Selected Derivatives

	physiochemical parameters						ADMET					bioavailability & drug-likeness				
no.	Log P[a]	M.Wt[b]	HBA[c]	HBD[d]	NROTB[e]	TPSA[f]	S[g]	HIA[h]	BBB[i]	CYP3A4 inhibitor	CYP2D6 inhibitor	LD_{50}[j]	hepatotoxicity	Lipinski[k]	Veber[l]	Muegge[m]	Ghose[n]	PAINS[o]
3c	1.04	250.23	4	1	2	117.29	654	high	no	no	no	1000	no	yes	yes	yes	yes	0
6a	2.08	326.21	2	0	4	62.68	9.76	high	yes	no	no	1000	no	yes	yes	yes	yes	0
6e	2.99	463.18	3	0	8	71.91	0.28	high	yes	yes	no	1000	no	yes	yes	yes	yes	0

[a]Log P: logarithm of the compound partition coefficient between *n*-octanol and water. [b]M.Wt: molecular weight. [c]HBA: number of hydrogen bond acceptors. [d]HBD: number of hydrogen bond donors. [e]NROTB: number of rotatable bonds. [f]TPSA: polar surface area. Drug-like TPSA < 140−150 A^2. [g]S: aqueous solubility (mg/L). [h]HIA: human intestinal absorption. [i]BBB: blood−brain barrier penetration. [j]LD_{50}: the median lethal dose (mg/kg). Toxicity classes according to GHS are Class I: fatal if swallowed ($LD_{50} \leq 5$), Class II: fatal if swallowed ($5 < LD_{50} \leq 50$), Class III: toxic if swallowed ($50 < LD_{50} \leq 300$), Class IV: harmful if swallowed ($300 < LD_{50} \leq 2000$), Class V: may be harmful if swallowed ($2000 < LD_{50} \leq 5000$), and Class VI: nontoxic ($LD_{50} > 5000$). [52] [k]Lipinski rule: log P ≤ 5, M.Wt ≤ 500 Da, HBA ≤ 10, and HBD ≤ 5. [48] [l]Veber rule: NROTB ≤ 10 and TPSA ≤ 140. [49] [m]Muegge rule: −2 ≤ log P ≤ 5, 200 ≤ M.Wt ≤ 600 Da, TPSA ≤ 150, Num. rings ≤ 7, Num. carbons> 4, Num. heteroatom > 1, NROTB ≤ 15, HBA ≤ 10, and HBD ≤ 5. [50] [n]Ghose rule: 160 ≤ M.Wt ≤ 480 Da, −0.4 ≤ log P ≤ 5.8, 20 ≤ atoms ≤ 70, 40 ≤ MR ≤ 130. [51]

https://doi.org/10.1021/acsomega.2c02410
ACS Omega 2022, 7, 21267−21279

seen in the case of N3-substitution with 3-allyl **4c**, 3-ethylacetate **5c**, 3-hydroxypropyl **7c**, or 3-bromopropyl **6c** groups, whereas other derivatives and the parent unsubstituted thiazolidine-2,4-dione **1** showed moderate anticancer activities against the screened cell line with relatively slight differences in activities when compared.

Mechanistic studies revealed that the *N*3-3-bromopropyl TZD **6a** exhibited the highest inhibitory potentials of SOD, ALDHA1, and GPX among the elected hits. The TZD derivatives bearing 4-nitrobenzylidene **3c** and the 5-(4-(3-bromopropoxy)benzylidene)-3-(3-bromopropyl) thiazolidine-2,4-dione **6e** were nearly equipotent. These results were correlated with the TZD derivatives' potential to induce cellular ROS content following Caco-2 cells' treatment with IC_{50} doses. However, *in vitro* evaluation of SOD showed that the (3-bromopropoxy)benzylidene derivative **6e** was slightly more potent than the *N*3-3-bromopropyl TZD **6a** precursor.

4. CONCLUSIONS

The current study portrays the utility of TZD-based SOD inhibitors endowed with ALDH and GPX inhibitory potentials to harness oxidative stress for combating colorectal cancer. Interestingly, all of the designed TZDs were safe on normal human cells (EC_{100} approaching 47.5-folds higher than doxorubicin). The hit derivatives **3c, 6a**, and **6e** (IC_{50} = 4.4−4.7 μM) were superior to doxorubicin against Caco-2 cells. They exhibited modest SOD inhibition (IC_{50} = 97.2−228.8 μM). On a cellular level, the IC_{50} doses of the hit derivatives **3c, 6a**, and **6e** promoted ROS-induced oxidative stress by 21.42, 7.863, and 8.986-folds *via* suppression of the antioxidant activities of SOD, ALDH1A, and GPX up to 70.1, 95.84, and 87.03%, respectively, in the treated Caco-2 cells. Docking simulations displayed their possible binding modes and essential structural features. Their computed physicochemical parameters and pharmacokinetic profiles highlighted acceptable drug-like properties. Accordingly, the oxidative stress-based anticancer therapeutics launch an opportunity to improve our ability to introduce novel strategies for combating cancer.

5. EXPERIMENTAL SECTION

5.1. Chemistry. *5.1.1. General Methods and Instruments.* Melting points were uncorrected and observed using the Mel-Temp apparatus. Reactions were monitored using thin-layer chromatography (TLC) (aluminum plates of silica gel; Kiesel gel G, Merk). Ultraviolet light (UV 254 nm) was used in visualization. Sonication was carried out using an Ultrasonic Cleaner model UD50SH-2LQ. IR spectra were determined using a Bruker Tensor 37 FTIR spectrophotometer. NMR spectroscopic analysis was carried out using JEOL ECA 500, NMR unit, Mansoura University, Egypt. Chemical shifts are reported in ppm and coupling constants (*J*) in Hz (Hertz) (abbreviations used in the spectra: s = singlet, d = doublet, t = triplet, q = quartet, m = multiple, dd = double of doublets). Microanalysis was established at the Faculty of Science, El Azhar University, Egypt.

5.2. General Procedure for the Preparation of 5-Arylidine-2,4-thiazolidinediones. A mixture of **1** (0.085 mol) and sodium acetate (0.69 g, 0.085 mol) in ethanol (30 mL) was refluxed with aromatic aldehydes (0.085 mol) for 3−15 h. The precipitate obtained was filtered off and washed with methanol.

*5.2.1. 5-Benzylidenethiazolidine-2,4-dione (**3a**).* It was obtained as a pale yellow powder, in 64% yield; mp = 238 °C (Lit. mp[53] = 240−241 °C).

*5.2.2. 5-(3-Chlorobenzylidene)thiazolidine-2,4-dione (**3b**).* It was obtained as a white crystal, in 60% yield; mp = 272 °C (Lit. mp[53] = 270−271 °C).

*5.2.3. 5-(4-Nitrobenzylidene)thiazolidine-2,4-dione (**3c**).* It was obtained as a pale yellow powder, in 71% yield; mp = 220 °C (Lit. mp[54] = 220−223 °C).

*5.2.4. 5-(4-(Dimethylamino)benzylidene)thiazolidine-2,4-dione (**3d**).* It was obtained as an orange powder, in 86% yield; mp = 279 °C (Lit. mp[55] = 281−282 °C).

*5.2.5. 5-(4-Hydroxybenzylidene)thiazolidine-2,4-dione (**3e**).* It was obtained as a yellow crystal, in 56% yield; mp = 278 °C (Lit. mp[53] = 280−281 °C).

5.3. General Procedure for the Synthesis of *N*-Alkyl 5-arylidene-2,4-thiazolidinediones. A mixture of 5-arylidine-2,4-thiazoldinedione **7**−**11** (1 mmol) and anhydrous potassium carbonate (0.49 g, 1.2 mmol) in DMF (15 mL) was stirred for 15 min, then the alkyl halide (1.2 mmol) was added. The reaction mixture was irradiated under ultrasound irradiation for 20 to 60 min till the end of the reaction, as monitored by TLC. The mixture was poured on to crushed ice and the precipitate obtained was filtered off, washed with water, dried, and recrystallized from ethanol.

*5.3.1. 3-Allyl-5-(substituted benzylidene)thiazolidene-2,4-diones (4). 5.3.1.1. 3-Allyl-5-benzylidenethiazolidine-2,4-dione (**4a**).* It was obtained as a white powder, in 64% yield, mp = 98 °C (Lit. mp[40] = 101−103 °C), R_f = 0.69 (ethylacetate/*n*-hexane, 1:3). IR (KBr) υ (cm^{-1}): 1733 (C=O), 1685 (C=O), 1607 (C=C), 1115 (C-N). ^{1}H NMR ($CDCl_3$, 400 MHz) δ_H ppm; 7.94 (s, 1 H, Ph-C<u>H</u>=C), 7.55−7.44 (m, 5 H, Ar-H), 5.93−5.83 (m, 1 H, $CH_2C\underline{H}=CH_2$), 5.35, 5.30 (2 d, 2 H, *J* = 4.0 Hz, *J* = 12.0 Hz, *J* = 16.0 Hz, HC=C<u>H</u>$_2$), 4.39 (d, 2 H, *J* = 8.0 Hz, CH_2-N); Figure S1. ^{13}C NMR ($CDCl_3$, 100 MHz) δ_C ppm; 167.5, 165.9 (2 C=O), 134.0 (Ph-<u>C</u>H=C), 133.2 (Ar-C), 130.6 (<u>C</u>H=CH_2), 130.2, 129.2 (Ar-C), 121.4 (CH=<u>C</u>), 119.0 (HC=<u>C</u>H_2), 43.8 (N-CH_2); Figure S2. Anal. calcd for $C_{13}H_{11}NO_2S$: C, 63.65; H, 4.98; N, 5.32; S, 13.07. Found C, 63.62; H, 4.50; N, 5.35; S, 13.09.

*5.3.1.2. 3-Allyl-5-(3-chlorobenzylidene)thiazolidine-2,4-dione (**4b**).* It was obtained as pale yellow needles, yield (60%), mp = 210 °C, R_f = 0.86 (ethylacetate/*n*-hexane, 1:3). IR (KBr) υ (cm^{-1}): 1736 (C=O), 1675 (C=O), 1606 (C=C), 1110 (C-N). ^{1}H NMR ($CDCl_3$, 400 MHz) δ_H ppm; 7.85 (s, 1 H, Ar-C<u>H</u>=C), 7.50 (s, 1 H, Ar-H), 7.43 (m, 3 H, Ar-H), 5.92−5.83 (m, 1 H, C<u>H</u>=CH_2), 5.35, 5.30 (2 d, 2 H, HC=C<u>H</u>$_2$), 4.38 (d, 2 H, CH_2-N); Figure S3. ^{13}C NMR ($CDCl_3$, 100 MHz) δ_C ppm; 167.0, 165.6 (2 C=O), 135.3 (Ph-<u>C</u>H=C), 134.9 (Ar-C), 132.2 (<u>C</u>H=CH_2), 130.5, 130.4, 130.0, 127.9 (Ar-C), 123.1 (CH=<u>C</u>), 119.2 (HC=<u>C</u>H_2), 43.9 (N-CH_2); Figure S4. Anal. calcd for $C_{13}H_{10}ClNO_2S$: C, 55.82; H, 3.60; N, 5.01; S, 11.46. Found C, 55.81; H, 3.57; N, 5.11; S, 11.44.

*5.3.1.3. 3-Allyl-5-(4-nitrobenzylidene)thiazolidine-2,4-dione (**4c**).* It was obtained as a yellow powder, 52% yield, mp = 159 °C, R_f = 0.79 (ethylacetate/*n*-hexane, 1:3). IR (KBr) υ (cm^{-1}): 1738 (C=O), 1678 (NC=O), 1606 (C=C), 1515, 1345 (NO_2), 1111 (C-N). ^{1}H NMR ($CDCl_3$, 400 MHz) δ_H ppm; 8.36 (d, 2 H, *J* = 8 Hz Ar-H), 7.95 (s, 1 H, Ar-C<u>H</u>=C), 7.70 (d, 2 H, Ar-H), 5.93−5.83 (m, 1 H, $CH_2C\underline{H}=CH_2$), 5.36−5.29 (m, 2 H, HC=C<u>H</u>$_2$), 4.40 (d, 2 H, *J* = 4 Hz, CH_2-

https://doi.org/10.1021/acsomega.2c02410
ACS Omega 2022, 7, 21267−21279

N); Figure S5. ^{13}C NMR ($CDCl_3$, 100 MHz) δ_C ppm; 166.3, 165.3 (2× C═O), 148.0 (Ar-C), 139.2 (Ph-CH═C), 130.66 (CH═CH_2), 130.65, 129.7 (Ar-C), 126.07 (CH═C), 124.41 (Ar-C), 119.5 (HC═CH_2), 44.2 ((N-CH_2); Figure S6. Anal. calcd for $C_{13}H_{10}N_2O_4S$: C, 53.79; H, 3.47; N, 9.65; S, 11.04. Found C, 53.75; H, 3.46; N, 9.62; S, 11.07.

5.3.1.4. 3-Allyl-5-(4-(dimethylamino)benzylidene)-thiazolidine-2,4-dione (4d). It was obtained as a yellow crystal, 58% yield, mp = 228 °C, R_f = 0.54 (ethylacetate/*n*-hexane, 1:3). IR (KBr) υ (cm^{-1}): 1728 (C═O), 1672 (NC═O), 1590 (C═C), 1110 (C-N). ^{1}H NMR ($CDCl_3$, 400 MHz) δ_H ppm; 7.85 (s, 1 H, Ar-CH═C), 7.44−7.42 (d, 2 H, *J* = 8 Hz, Ar-H), 6.78−6.76 (d, 2 H, *J* = 8 Hz, Ar-H), 5.93−5.83 (m, 1 H, CH_2CH═CH_2), 5.32, 5.23 (2 d, 2 H, HC═CH_2), 4.37 (d, 2 H, *J* = 8 Hz, CH_2-N), 3.09 (s, 6 H, 2 CH_3); Figure S7. ^{13}C NMR ($CDCl_3$, 100 MHz) δ_C ppm; 168.1, 166.4 (2 C═O), 151.3 (Ar-C), 134.8 (Ph-CH═C), 132.5(N-CH═CH_2), 132.1, 130.5, 121.1 (Ar-C), 118.6 (HC═CH_2), 118.5 (CH═C), 114.5, 113.3 (Ar-C), 112.2 (N-CH_2), 43.6, 40.2 (2 CH_3); Figure S8. Anal. calcd for $C_{15}H_{16}N_2O_2S$: C, 62.48; H, 5.59; N, 9.71; S, 11.12. Found C, 62.43; H, 5.56; N, 9.69; S, 11.11.

5.3.1.5. 3-Allyl-5-(4-(allyloxy)benzylidene)thiazolidine-2,4-dione (4e). It was obtained as a white powder, 65% yield, mp = 81 °C, R_f = 0.73 (ethylacetate/*n*-hexane, 1:3). IR (KBr) υ (cm^{-1}): 1739 (C═O), 1685 (NC═O), 1595 (C═C), 1181.1 (C-O), 1110 (C-N). ^{1}H NMR ($CDCl_3$, 400 MHz) δ_H ppm; 7.88 (s, 1 H, Ar-CH═C), 7.49−7.47 (d, 2 H, *J* = 8 Hz, Ar-H), 7.03−7.01 (d, 2 H, *J* = 8Hz, Ar-H), 6.11−6.03 (m, 1 H, OCH_2CH═CH_2), 5.91−5.83 (m, 1 H, NCH_2CH═CH_2), 5.48, 5.43, 5.36, 5.25 (4 d, 4 H, O-, N-HC═CH_2), 4.63 (d, 2 H, *J* = 4 Hz, OCH_2), 4.37 (d, 2 H, *J* = 4 Hz, NCH_2); Figure S9. ^{13}C NMR ($CDCl_3$, 100 MHz) δ_C ppm; 167.7, 166.1 (2 C═O), 160.5 (Ar-C), 133.8 (Ph-CH═C), 132.4 (OCH_2-CH═CH_2), 132.3 (Ar-C), 130.3 (NCH_2-CH═CH_2), 125.9 (Ar-C), 118.8 (OCH_2-CH═CH_2), 118.4 (HC═CH_2), 118.3 (NCH_2-CH═CH_2), 115.5 (Ar-C), 68.9 (OCH_2CH═CH_2), 43.8 (NCH_2CH═CH_2); Figure S10. Anal. calcd for $C_{16}H_{15}NO_3S$: C, 63.77; H, 5.02; N, 4.65; S, 10.64. Found C, 63.74; H, 5.06; N, 4.64; S, 10.62.

*5.3.2. Synthesis of Ethyl-2-(5-substituted benzylidene-2,4-dioxothiazolidin-3-yl)acetate (5). 5.3.2.1. Ethyl-2-(5-benzylidene-2,4-dioxothiazolidin-3-yl)acetate (**5a**).* It was obtained as colorless crystals, 79% yield, mp = 92 °C (Lit. mp[56] 75−77 °C), R_f = 0.61 (ethylacetate/*n*-hexane, 1:3). IR (KBr) υ (cm^{-1}): 1741 (C═O), 1684 (NC═O), 1605 (C═C), 1219 (C-N), 1152 (C-O). ^{1}H NMR ($CDCl_3$, 400 MHz) δ_H ppm; 7.96 (s, 1 H, Ph-CH═C), 7.55−7.47 (m, 5 H, Ar-H), 4.50 (s, 2 H, NCH_2), 4.27 (q, 2 H, OCH_2CH_3), 1.32 (t, 3 H, OCH_2CH_3); Figure S11. ^{13}C NMR ($CDCl_3$, 100 MHz) δ_C ppm; 167.5, 166.2, 165.6 (3× C═O), 134.7 (Ph-CH═C), 133.1, 130.8, 130.3, 129.3 (Ar-C), 121.0 (-CH═C), 62.2 (OCH_2CH_3), 42.1 (NCH_2), 14.1 (OCH_2CH_3); Figure S12. Anal. calcd for $C_{14}H_{13}NO_4S$: C, 57.72; H, 4.50; N, 4.81; S, 11.01. Found C, 57.76; H, 4.48; N, 4.80; S, 10.98.

*5.3.2.2. Ethyl-2-(5-(4-nitrobenzylidene)-2,4-dioxothiazolidin-3-yl)acetate (**5c**).* It was obtained as yellow needles, 62% yield, mp = 139 °C, R_f = 0.71 (ethylacetate/*n*-hexane, 1:3). IR (KBr) υ (cm^{-1}): 1734 (C═O), 1697 (NC═O), 1609 (C═C), 1535, 1344 (NO_2), 1235 (C-N), 1149 (C-O). ^{1}H NMR ($CDCl_3$, 400 MHz) δ_H ppm; 8.28 (d, 2 H, *J* = 8 Hz, Ar-H), 7.89 (s, 1 H, Ph-CH═C), 7.62 (d, 2 H, Ar-H), 4.43 (s, 2 H, NCH_2), 4.20 (q, 2 H, *J* = 8 Hz, OCH_2CH_3), 1.24 (t, 3 H, *J* = 8 Hz, OCH_2CH_3); Figure S13. ^{13}C NMR ($CDCl_3$, 100 MHz) δ_C ppm; 166.3, 166.0, 165.0 (3× C═O), 148.1 (Ar-C), 139.1 ((Ph-CH═C), 131.3, 130.7, 125.6 (Ar-C), 124.4 (-CH═C), 62.4 (OCH_2CH_3), 44.3 (NCH_2), 14.1 (OCH_2CH_3); Figure S14. Anal. calcd for $C_{14}H_{12}N_2O_6S$: C, 50.00; H, 3.60; N, 8.33; S, 9.53. Found C, 49.97; H, 3.65; N, 8.31; S, 9.55.

*5.3.2.3. Ethyl-2-(5-(4-(dimethylamino)benzylidene)-2,4-dioxothiazolidin-3-yl)acetate (**5d**).* It was obtained as orange crystals, yield (79%), mp = 170 °C (Lit. mp[56] = 170−171 °C), R_f = 0.5 (ethylacetate/*n*-hexane, 1:3). IR (KBr) υ (cm^{-1}): 1729 (C═O), 1676 (NC═O), 1589 (C═C), 1220 (C-N), 1147 (C-O). ^{1}H NMR ($CDCl_3$, 400 MHz) δ_H ppm; 7.87 (s, 1 H, Ar-CH═C), 7.45 (d, 2 H, *J* = 8.8 Hz, Ar-H), 6.78 (d, 2 H, *J* = 12 Hz, Ar-H), 4.48 (s, 2 H, NCH_2), 4.26 (q, 2 H, *J* = 7.2 Hz, OCH_2CH_3), 3.09 (s, 6 H, N, N-2× CH_3), 1.31 (t, 3 H, *J* = 7.2 Hz, OCH_2CH_3); Figure S15. ^{13}C NMR ($CDCl_3$, 100 MHz) δ_C ppm; 168.1, 166.5, 166.0 (3 C═O), 151.4 (Ar-C), 135.5 (Ph-CH═C), 132.6, 120.9 (Ar-C), 114.0 (Ph-CH═C), 112.2 (Ar-C), 62.0 (OCH_2CH_3), 42.0 (NCH_2), 40.2 (2× NCH_3), 14.1 (OCH_2CH_3); Figure S16. Anal. calcd for $C_{16}H_{18}N_2O_4S$: C, 57.47; H, 5.43; N, 8.38; S, 9.59. Found C, 57.46; H, 5.33; N, 8.41; S, 9.55.

*5.3.2.4. Ethyl-2-(5-(4-(2-ethoxy-2-oxoethoxy)-benzylidene)-2,4-dioxothiazolidin-3-yl)acetate (**5e**).* It was obtained as yellow crystals, 51% yield, mp = 86 °C (Lit. mp[42] = 115 °C), R_f = 0.47 (ethylacetate/*n*-hexane, 1:3). IR (KBr) υ (cm^{-1}): 1741 (C═O), 1688 (NC═O), 1592 (C═C), 1209 (C-N), 1148.25 (C-O). ^{1}H NMR ($CDCl_3$, 400 MHz) δ_H ppm; 7.90 (s, 1 H, Ar-CH═C), 7.51 (d, 2 H, *J* = 8 Hz, Ar-H), 7.03 (d, 2 H, *J* = 8 Hz, Ar-H), 4.70 (s, 2 H, O-CH_2), 4.49 (s, 2 H, N-CH_2), 4.33−4.24 (qq, 4 H, O-CH_2-CH_3), 1.35−1.30 (dd, 6 H, 2× CH_3); Figure S17. ^{13}C NMR ($CDCl_3$, 100 MHz) δ_C ppm; 168.2, 167.5, 166.3, 165.7 (4× C═O), 159.6 (Ar-C-O), 134.2 (Ph-CH═C), 132.33 (Ar-C), 126.71 (Ar-C), 118.7 (Ph-CH═C), 115.4 (Ar-C), 65.2 (O-CH_2), 62.1 (O-(O-CH_2-CH_3)), 61.6 (N-(O-CH_2-CH_3)), 42.1 (N-CH_2), 14.19 (O-(O-CH_2-CH_3)), 14.11 (N-(O-CH_2-CH_3)); Figure S18. Anal. calcd for $C_{18}H_{19}NO_7S$: C, 54.95; H, 4.87; N, 3.56; S, 8.18. Found C, 54.92; H, 4.86; N, 3.55; S, 8.16.

*5.3.3. Synthesis of 3-(3-Bromopropyl)-5-(substituted benzylidene)thiazolidine-2,4-dione (6). 5.3.3.1. 5-Benzylidene-3-(3-bromopropyl)thiazolidine-2,4-dione (**6a**).* It was obtained as colorless crystals, 60% yield, mp = 118 °C, R_f = 0.68 (ethylacetate/*n*-hexane, 1:3). IR (KBr) υ (cm^{-1}): 1745 (C═O), 1684 (C═O), 1609.(C═C), 1232 (C-N). ^{1}H NMR ($CDCl_3$, 400 MHz) δ_H ppm; 7.95 (s, 1 H, Ph-CH═C), 7.54−7.46 (m, 5 H, Ar-H), 3.94 (t, 2 H, NCH_2), 3.44 (t, 2 H, NCH_2-CH_2-CH_2), 2.28 (quintet, 2 H, CH_2-CH_2-CH_2,); Figure S19. ^{13}C NMR ($CDCl_3$, 100 MHz) δ_C ppm; 167.92, 166.29, (2 C═O), 134.22, (CH═C), 133.16, 130.68, 130.28, 129.28, (Ar-C), 121.20, (CH═C), 40.69 (NCH_2), 30.8 (NCH_2-CH_2-CH_2), 29.48 (CH_2-CH_2-CH_2); Figure S20. Anal. calcd for $C_{23}H_{18}N_2O_4S_2$: C, 61.32; H, 4.03; N, 6.22; S, 14.23. Found C, 61.31; H, 4.01; N, 6.21; S, 14.22.

*5.3.3.2. 3-(3-Bromopropyl)-5-(4-nitrobenzylidene)-thiazolidine-2,4-dione (**6c**).* It was obtained as a yellow powder, 49% yield, mp = 128 °C, R_f = 0.60 (ethylacetate/*n*-hexane, 1:3). IR (KBr) υ (cm^{-1}): 1748 (C═O), 1691 (NC═O), 1606 (C═C), 1516−1346 (NO_2), 1130 (C-N), 685 (C-Br). ^{1}H NMR ($CDCl_3$, 400 MHz) δ_H ppm; 8.37 (d, 2 H, *J* = 12 Hz, Ar-H), 7.95 (s, 1 H, Ph-CH═C), 7.70 (d, 2 H, *J* = 8 Hz, Ar-H), 3.96 (t, 2 H, NCH_2), 3.44 (t, 2H, $BrCH_2$), 2.29 (pentet, 2 H, $CH_2CH_2CH_2$); Figure S21. ^{13}C NMR ($CDCl_3$, 100 MHz) δ_C ppm; 167.5, 165.9 (2× C═O), 148.03 (CH═

https://doi.org/10.1021/acsomega.2c02410
ACS Omega 2022, 7, 21267−21279

C), 139, 131.4, 130.4 (Ar-C), 126.5 (CH=C), 124.83 (Ar-C), 40.9 (NCH$_2$), 32.1 (BrCH$_2$), 30.7 (N-CH$_2$-CH$_2$-CH$_2$), Figure S22. Anal. calcd for $C_{13}H_{11}BrN_2O_4S$: C, 42.06; H, 2.99; N, 7.55; S, 8.64. Found C, 42.11; H, 2.94; N, 7.54; S, 8.66.

5.3.3.3. 3-(3-Bromopropyl)-5-(4-(dimethylamino)-benzylidene)thiazolidine-2,4-dione ***(6d)***. It was obtained as yellow crystals, 63% yield, mp = 160 °C, R_f = 0.62 (ethylacetate/*n*-hexane, 1:3). IR (KBr) υ (cm^{-1}): 1724 (C=O), 1674 (C=O), 1581 (C=C),1189 (C-N), 520 (C-Br). ^{1}H NMR (CDCl$_3$, 400 MHz) δ_H ppm; 7.86 (s, 1 H, Ar-CH=C), 7.46 (d, 2 H, *J* = 8 Hz, Ar-H), 6.86−6.81 (m, 2 H, Ar-H), 3.92 (t, 2 H, NCH$_2$), 3.43 (t, 2 H, BrCH$_2$), 3.1 (s, 6 H, 2× N-CH$_3$), 2.27 (quintet, 2 H, CH$_2$-CH$_2$-CH$_2$); Figure S23. ^{13}C NMR (DMSO-d_6, 100 MHz) δ_C ppm; 168.1, 166.3 (2× C=O), 152.0 (Ar-C), 134.3 (CH=C), 134.3, 132.8, 130.5, 120.2 (Ar-C), 113.8 (CH=C), 112.5 (Ar-C), 58.9 (N-CH$_2$), 40.09, 40.17 (2× CH$_3$), 32.2 (CH$_2$-CH$_2$-CH$_2$), 30.8 (CH$_2$-CH$_2$-CH$_2$); Figure S24. Anal. calcd for $C_{15}H_{17}BrN_2O_2S$: C, 48.79; H, 4.64; N, 7.59; S, 8.68. Found C, 48.75; H, 4.66; N, 7.55; S, 8.65.

5.3.3.4. 5-(4-(3-Bromopropoxy)benzylidene)-3-(3-bromopropyl)thiazolidine-2,4-dione ***(6e)***. It was obtained as a yellow precipitate, 35% yield, mp = 92 °C, R_f = 0.49 (ethylacetate/*n*-hexane, 1:3). IR (KBr) υ (cm^{-1}): 1738 (C=O), 1680 (NC=O), 1598 (C=C), 1258 (C-O), 1127 (C-N).^{1}H NMR (CDCl$_3$, 400 MHz) δ_H ppm; 7.88 (s, 1 H, CH=C), 7.50 (d, 2 H, *J* = 8 Hz, Ar-H), 7.03 (d, 2 H, Ar-H), 4.20 (t, 2 H, O-CH$_2$CH$_2$CH$_2$), 3.92 (t, 2 H, N-CH$_2$CH$_2$CH$_2$), 3.63 (t, 2 H, N-CH$_2$CH$_2$CH$_2$), 3.43 (t, 2 H, O-CH$_2$CH$_2$CH$_2$), 2.37 (quintet, 2 H,O-CH$_2$CH$_2$CH$_2$), 2.27 (quintet, 2 H, N-CH$_2$CH$_2$CH$_2$); Figure S25. ^{13}C NMR (CDCl$_3$, 100 MHz) δ_C ppm; 168.1, 166.4 (2× C=O), 160.6 (Ar-C), 134.0 (CH=C), 132.3 (Ar-C), 126.0 (Ar-C), 115.30 (Ar-C), 114.8 (CH=C), 65.5 (OCH$_2$) 40.6 (NCH$_2$), 32.1, 30.8 (2× CH$_2$Br), 29.7, 29.5 (CH$_2$CH$_2$CH$_2$); Figure S26. Anal. calcd for $C_{26}H_{23}BrN_2O_6S_2$: C, 51.75; H, 3.84; N, 4.64; S, 10.62. Found C, 51.73; H, 3.81; N, 4.65; S, 10.65.

5.3.4. 3-(3-Hydroxypropyl)-5-(substituted benzylidene)-thiazolidine-2,4-dione (7). 5.3.4.1. 5-Benzylidene-3-(3-hydroxypropyl)thiazolidine-2,4-dione ***(7a)***. It was obtained as colorless crystals, 65% yield, mp = 110 °C, R_f = 0.34 (ethylacetate/*n*-hexane, 1:3). IR (KBr) υ (cm^{-1}): 3428 (OH), 1757 (C=O), 1698 (NC=O), 1610 (C=C), 1112 (C-N). ^{1}H NMR (CDCl$_3$, 400 MHz) δ_H ppm; 7.95 (s, 1 H, CH=C), 7.55−7.47 (m, 5 H, Ar-H), 3.96 (t, 2 H, N-CH$_2$CH$_2$CH$_2$), 3.65 (t, 2 H, CH$_2$CH$_2$CH$_2$-OH), 2.15 (bs, 1 H, OH, D$_2$O exchangeable H), 1.92 (quintet, 2 H, CH$_2$CH$_2$CH$_2$); Figure S27. ^{13}C NMR (CDCl$_3$, 100 MHz) δ_C ppm; 168.5, 167.0 (2× C=O), 134.4 (CH=C), 133.1, 130.7, 130.3, 129.5, 129.3 (Ar-C), 121.1 (CH=C), 58.9 (CH$_2$OH), 38.5 (NCH$_2$), 30.6 (CH$_2$CH$_2$CH$_2$); Figure S28. Anal. calcd for $C_{13}H_{13}NO_3S$: C, 59.30; H, 4.89; N, 5.32; S, 12.18. Found C, 59.28; H, 4.88; N, 5.28; S, 12.13.

5.3.4.2. 3-(3-Hydroxypropyl)-5-(4-nitrobenzylidene)-thiazolidine-2,4-dione ***(7c)***. It was obtained as a brown powder, 55% yield, mp = 170 °C, R_f = 0.17 (ethylacetate:*n*-hexane, 1:3). IR (KBr) υ (cm^{-1}): 3451 (OH), 1738 (C=O), 1676 (NC=O), 1608 (C=C), 1510, 1345 (NO$_2$), 1106 (C-N). ^{1}H NMR (CDCl$_3$, 400 MHz) δ_H ppm; 8.37 (d, 2 H, *J* = 8 Hz, Ar-H), 8.04 (s, 1 H, CH=C), 7.91 (d, 2 H, Ar-H), 4.61 (t, 1 H, OH, D$_2$O exchangeable H), 3.74 (t, 2H, NCH$_2$), 3.47 (q, 2 H, CH$_2$OH), 1.75 (quintet, 2 H, CH$_2$CH$_2$CH$_2$); Figure S29. ^{13}C NMR (CDCl$_3$, 100 MHz) δ_C ppm; 167.3, 165.8 (2× C=O), 148.0 (Ar-C), 139.8 (CH=C), 131.5, 130.4 126.4 (CH=C), 124.8 (Ar-C), 58.9 (OCH$_2$), 30.6 (CH$_2$-CH$_2$-CH$_2$); Figure S30. Anal. calcd for $C_{13}H_{12}N_2O_5S$: C, 50.64; H, 3.92; N, 9.09; S, 10.40. Found C, 50.59; H, 3.91; N, 9.04; S, 10.37.

5.3.4.3. 5-(4-(Dimethylamino)benzylidene)-3-(3-hydroxypropyl)thiazolidine-2,4-dione ***(7d)***. It was obtained as a brown precipitate, yield (85%), mp = 154 °C, R_f = 0.43 (ethylacetate/*n*-hexane, 1:3). IR(KBr) υ (cm^{-1}): 3452 (OH), 1715.22 (C=O), 1645 (NC=O), 1585 (C=C), 1129 (C-N). ^{1}H NMR (CDCl$_3$, 400 MHz) δ_H ppm; 7.79 (s, 1 H, CH=C), 7.48 (d, 2 H, *J* = 12 Hz, Ar-H), 6.84 (d, 2 H, Ar-H), 4.58 (t, 1 H, OH, D$_2$O exchangeable H), 3.70 (t, 2 H, NCH$_2$), 3.45 (q, 2 H, CH$_2$OH), 3.03 (s, 6 H, 2× CH$_3$), 1.72 (quintet, 2 H, CH$_2$CH$_2$CH$_2$); Figure S31. ^{13}C NMR (CDCl$_3$, 100 MHz) δ_C ppm; 168.0, 166.3 (2× C=O), 152.0 (Ar-C), 134.3 (CH=C), 132.8, 120.2 (Ar-C), 113.8 (CH=C), 112.5 (Ar-C), 58.95 (CH$_2$OH), 40.06, 40.15 (NCH$_3$) under a solvent peak, 30.9 (CH$_2$CH$_2$CH$_2$); Figure S32. Anal. calcd for $C_{15}H_{18}N_2O_3S$: C, 58.80; H, 5.92; N, 9.14; S, 10.46. Found C, 58.79; H, 5.91; N, 9.11; S, 10.44.

5.4. Biological Evaluation. *5.4.1. Cytotoxicity Screening on Normal Human Cells.* The normal human lung fibroblast Wi-38 cell line was used to detect the cytotoxicity of the studied compounds via MTT assay as detailed in the Supporting Information.

5.4.2. Anticancer Screening. The anticancer effect of the abovementioned compounds was assayed using the colon cancer cell line Caco-2 via MTT assay as described in the Supporting Information.

5.4.3. SOD Inhibition Assay. SOD inhibition was assayed as detailed in the Supporting Information using the superoxide dismutase kit from R&D Systems according to the manufacturer's instructions.

5.4.4. Inhibition of the Antioxidant Enzymes in Colorectal Cancer Cells (Caco-2). After 72 h of incubation of Caco-2 cells with IC_{50} of the most effective anticancer compounds, the antioxidant enzyme activities (SOD, ALDH1, and GPX) were determined as previously reported,[57−59] as described in the Supporting Information.

5.4.5. Determination of Cellular Reactive Oxygen Species in Colorectal Cancer (Caco-2). The cellular reactive oxygen species (ROS) was determined by incubating the untreated and the most effective anticancer compounds-treated Caco-2 with 2′,7′-dichlorofluorescein diacetate (DCFDA), as detailed in the Supporting Information.

5.5. Molecular Modeling Studies. *5.5.1. Docking.* Docking simulations were performed by employing the Molecular Operating Environment (MOE) software package version 2015.10[45] as described in the Supporting Information.

5.5.2. In Silico Prediction of Physicochemical Properties, ADMET, and Drug-Likeness Parameters. Physicochemical properties, ADME. and drug-likeness were computed by *SwissADME*[47] software. Toxicity was predicted by PROTOX.[52]

■ ASSOCIATED CONTENT

Supporting Information

The Supporting Information is available free of charge at https://pubs.acs.org/doi/10.1021/acsomega.2c02410.

^{1}H- and ^{13}C NMR spectra of all the synthesized compounds are included, also, detailed biological evaluation and docking studies (PDF)

https://doi.org/10.1021/acsomega.2c02410
ACS Omega 2022, 7, 21267−21279

AUTHOR INFORMATION

Corresponding Author

Laila Fathy Awad − *Chemistry Department, Faculty of Science, Alexandria University, Alexandria 21321, Egypt;* orcid.org/0000-0001-9521-5511; Email: laila.fathy@yahoo.com

Authors

Mohamed Nabil Abd Al Moaty − *Chemistry Department, Faculty of Science, Alexandria University, Alexandria 21321, Egypt;* orcid.org/0000-0003-2843-9704

El Sayed H. El Ashry − *Chemistry Department, Faculty of Science, Alexandria University, Alexandria 21321, Egypt;* orcid.org/0000-0001-5480-239X

Asmaa Mostafa − *Chemistry Department, Faculty of Science, Alexandria University, Alexandria 21321, Egypt*

Marwa M. Abu-Serie − *Medical Biotechnology Department, Genetic Engineering and Biotechnology Research Institute, City of Scientific Research and Technological Applications (SRTA-City), Alexandria 21934, Egypt*

Mohamed Teleb − *Department of Pharmaceutical Chemistry, Faculty of Pharmacy, Alexandria University, Alexandria 21521, Egypt*

Complete contact information is available at: https://pubs.acs.org/10.1021/acsomega.2c02410

Notes

The authors declare no competing financial interest.

ACKNOWLEDGMENTS

The authors thank Alexandria University for its support.

REFERENCES

(1) Hanahan, D.; Weinberg, R. A. Hallmarks of cancer: the next generation. *Cell* **2011**, *144*, 646−674.

(2) Azad, M. B.; Chen, Y.; Gibson, S. B. Regulation of autophagy by reactive oxygen species (ROS): implications for cancer progression and treatment. *Antioxid. Redox Signaling* **2009**, *11*, 777−790.

(3) Sosa, V.; Moliné, T.; Somoza, R.; Paciucci, R.; Kondoh, H.; Leonart, M. E. Oxidative stress and cancer: an overview. *Ageing Res. Rev.* **2013**, *12*, 376−390.

(4) Sashi Papu John, A. M.; Ankem, M. K.; Damodaran, C. Oxidative Stress: A Promising Target for Chemoprevention. *Curr. Pharmacol. Rep.* **2016**, *2*, 73−81.

(5) Thapa, D.; Ghosh, R. Antioxidants for prostate cancer chemoprevention: Challenges and opportunities. *Biochem. Pharmacol.* **2012**, *83*, 1319−1330.

(6) Mohsenzadegan, M.; Farhad, S.; Mohammad, M. F.; Majid, K. Anti-Oxidants as Chemopreventive Agents in Prostate Cancer: A Gap Between Preclinical and Clinical Studies. *Recent Pat. Anti-Cancer Drug Discovery* **2018**, *13*, 224−239.

(7) Wattenberg, L. W. Chemoprevention of cancer. *Cancer Res.* **1985**, *45*, 1−8.

(8) Piccolella, S.; Pacifico, S. Plant-derived polyphenols: a chemopreventive and chemoprotectant worth-exploring resource in toxicology. *Adv. Mol. Toxicol.* **2015**, 161−214.

(9) Postovit, L.; Widmann, C.; Huang, P.; Gibson, S. B. Harenssing Oxidative Stress as an Innovative Target for Cancer Therapy. *Oxid. Med. Cell. Longevity* **2018**, *2018*, No. 6135739.

(10) Pani, G.; Colavitti, R.; Bedogni, B.; Fusco, S.; Ferraro, D.; Borrello, S.; Galeotti, T. Mitochondrial superoxide dismutase: a promising target for new anticancer therapies. *Curr. Med. Chem.* **2004**, *11*, 1299−1308.

(11) McCord, J. M.; Fridovich, I. Superoxide dismutase. An enzymic function for erythrocuprein (hemocuprein). *J. Biol. Chem.* **1969**, *244*, 6049−6055.

(12) Margis, R.; Dunand, C.; Teixeira, F. K.; Margis-Pinheiro, M. Glutathione peroxidase family−an evolutionary overview. *FEBS J.* **2008**, *275*, 3959−3970.

(13) Younus, H. Therapeutic potentials of superoxide dismutase. *Int. J. Health Sci.* **2018**, *12*, 88−93.

(14) Culotta, V. C.; Yang, M.; O'Halloran, T. V. Activation of superoxide dismutases: putting the metal to the pedal. *Biochim. Biophys. Acta, Mol. Cell Res.* **2006**, *1763*, 747−758.

(15) Irawan, B.; Labeda, I.; Lusikooy, R. E.; Sampetoding, S.; Kusuma, M. I.; Uwuratuw, J. A.; Syarifuddin, E.; Faruk, M.; et al. Association of superoxide dismutase enzyme with staging and grade of differentiation colorectal cancer: a cross-sectional study. *Ann. Med. Surg.* **2020**, *58*, 194−199.

(16) Li, S.; Fu, L.; Tian, T.; Deng, L.; Li, H.; Xiao, W.; Gong, Q. Disrupting SOD1 activity inhibits cell growth and enhances lipid accumulation in nasopharyngeal carcinoma. *Cell Commun. Signaling* **2018**, *16*, No. 28.

(17) Mulder, T. P.; Verspaget, H. W.; Janssens, A. R.; De Bruin, P. A.; Griffioen, G.; Lamers, C. B. Neoplasia-related changes of two copper (Cu)/zinc (Zn) proteins in the human colon. *Free Radical Biol. Med.* **1990**, *9*, 501−506.

(18) Skórska, K. B.; Płaczkowska, S.; Prescha, A.; Porębska, I.; Kosacka, M.; Pawełczyk, K.; Zabłocka-Słowińska, K. Serum Total SOD Activity and SOD1/2 Concentrations in Predicting All-Cause Mortality in Lung Cancer Patients. *Pharmaceuticals* **2021**, *14*, No. 1067.

(19) Miranda, A.; Janssen, L.; Bosman, C. B.; van Duijn, W.; Oostendorp-van de Ruit, M. M.; Kubben, F. J.; Griffioen, G.; Lamers, C. B.; Han, J.; Van Krieken, J. M.; van de Velde, C. J. Superoxide dismutases in gastric and esophageal cancer and the prognostic impact in gastric cancer. *Clin. Cancer Res.* **2000**, *6*, 3183−3192.

(20) Li, W.; Cao, L.; Han, L.; Xu, Q.; Ma, Q. Superoxide dismutase promotes the epithelial-mesenchymal transition of pancreatic cancer cells via activation of the H2O2/ERK/NF-κB axis. *Int. J. Oncol.* **2015**, *46*, 2613−2620.

(21) Marikovsky, M.; Nevo, N.; Vadai, E.; Harris-Cerruti, C. Cu/Zn superoxide dismutase plays a role in angiogenesis. *Int. J. Cancer* **2002**, *97*, 34−41.

(22) Mendes, F.; Pereira, E.; Martins, D.; Tavares-Silva, E.; Pires, A. S.; Abrantes, A. M.; Figueiredo, A.; Botelho, M. F. Oxidative stress in bladder cancer: an ally or an enemy? *Mol. Biol. Rep.* **2021**, *48*, 2791−2802.

(23) Arumsari, S.; Noor, D.; Dewi, S.; Syahrani, R.; Wanandi, S.In vitro transfectionof manganese superoxide dismutase small interfering RNA suppressesstemness of human breast cancer stem cells (aldehyde dehydrogenase1-positive): Focus on OCT4 mRNA expression and mammosphere-formingcapacity. *J. Nat. Sci., Biol. Med.* **2019**, *10*, S82−S87.

(24) Koppaka, V.; Thompson, D. C.; Chen, Y.; Ellermann, M.; Nicolaou, K. C.; Juvonen, R. O.; Petersen, D.; Deitrich, R. A.; Hurley, T. D.; Vasiliou, V. Aldehyde dehydrogenase inhibitors: A comprehensive review of the pharmacology, mechanism of action, substrate specificity, and clinical application. *Pharmacol. Rev.* **2012**, *64*, 520−539.

(25) Lowndes, S. A.; Adams, A.; Timms, A.; Fisher, N.; Smythe, J.; Watt, S. M.; Joel, S.; Donate, F.; Hayward, C.; Reich, S.; Middleton, M.; Mazar, A.; Harris, A. L. Phase I study of copper-binding agent ATN-224 in patients with advanced solid tumors Clin. *Cancer Res.* **2008**, *14*, 7526−7534.

(26) Lin, J.; Beer, T. M.; Ryan, C. J.; Mathew, P.; Wilding, G.; Morris, M.; Callahan, J. A.; Gordon, G.; Reich, S.; Carducci, M. A. A randomized, phase II study of ATN-224 in patients with biochemically relapsed, hormone-naive prostate cancer: a DOD/PCF Prostate Cancer Clinical Trials Consortium trial. *J. Clin. Oncol.* **2009**, *27*, No. 5135.

(27) Dong, X.; Zhang, Z.; Zhao, J.; Lei, J.; Chen, Y.; Li, X.; Chen, H.; Tian, J.; Zhang, D.; Liu, C.; Liu, C. The rational design of specific SOD1 inhibitors via copper coordination and their application in ROS signaling research. *Chem. Sci.* **2016**, *7*, 6251−6262.
(28) Somwar, R.; Shum, D.; Djaballah, H.; Varmus, H. Identification and preliminary characterization of novel small molecules that inhibit growth of human lung adenocarcinoma cells. *J. Biomol. Screen.* **2009**, *14*, 1176−1184.
(29) Somwar, R.; Erdjument-Bromage, H.; Varmus, H. E.; et al. Superoxide dismutase 1 (SOD1) is a target for a small molecule identified in a screen for inhibitors of the growth of lung adenocarcinoma cell lines. *Proc. Natl. Acad. Sci. U.S.A.* **2011**, *108*, 16375−16380.
(30) Kaminskyy, D.; Kryshchshyn, A.; Lesyk, R. 5-Ene-4-Thiazolidiononones-An efficient tool in medicinal chemistry. *Eur. J. Med. Chem.* **2017**, *140*, 542−594.
(31) Naim, M. J.; Alam, M. J.; Ahmed, S.; Nawaz, F.; Shrivastava, N.; Sahu, M.; Alam, O. Therapeutic journey of 2,4-thiazolidinedions as a versatile scaffold: An insight into structure activity relationship. *Eur. J. Med. Chem.* **2017**, *129*, 218−250.
(32) Munwar, S.; Lango, K. Thiazolidinediones (TZD) as a versatile scaffold in medicinal chemistry biological importance: A Review. *Int. J. Pharm. Sci. Rev.* **2020**, *63*, 58−70.
(33) Schweipert, M.; Jänsch, N.; Upadhyay, N.; Tilekar, K.; Wozny, E.; Basheer, S.; Wurster, E.; Müller, M.; CS, R.; Meyer-Almes, F. J. Mechanistic Insights into Binding of Ligands with Thiazolidinedione Warhead to Human Histone Deacetylase 4. *Pharmaceuticals* **2021**, *14*, No. 1032.
(34) Mueller, S. L.; Chrysanthopoulos, P. K.; Halili, M. A.; Hepburn, C.; Nebl, T.; Supuran, C. T.; Nocentini, A.; Peat, T. S.; Poulsen, S. A. The Glitazone Class of Drugs as Carbonic Anhydrase Inhibitors: A Spin-Off Discovery from Fragment Screening. *Molecules* **2021**, *26*, No. 3010.
(35) Mosmann, T. Rapid colorimetric assay for cellular growth and survival: application to proliferation and cytotoxicity assays. *J. Immunol. Methods* **1983**, *65*, 55−63.
(36) Lotfy, G.; Abdel Aziz, Y. M.; Aziz, Y. M. A.; Said, M. M.; El Ashry, E. S. H.; El Tamany, E. S. H.; Abu-Serie, M. M.; Abu-Serie, M. M.; Teleb, M.; Teleb, M.; Dömling, A.; Dömling, A.; Barakat, A. Molecular hybridization design and synthesis of novel spirooxindole-based MDM2 inhibitors endowed with BCL2 signaling attenuation; a step towards the next generation p53 activators. *Bioorg. Chem.* **2021**, *117*, No. 105427.
(37) Aziz, Y. M. A.; Lotfy, G.; Said, M. M.; El Ashry, E. S. H.; El Tamany, E. S. H.; Soliman, S.; Abu-Serie, M. M.; Teleb, M.; Yousuf, S.; Dömling, A. Design, synthesis, chemical and biochemical insights on to novel hybrid spirooxindoles-based p53-MDM2 inhibitors with potential Bcl2 signaling attenuation. *Front. Chem.* **2021**, *9*, No. 735236.
(38) Chadla, N.; Bahia, M. S.; Kaur, M.; Silakari, O. Thiazolidin-2,4-dione derivatives: Programmed chemical weapons for key protein targets of various pathological conditions. *Bioorg. Med. Chem.* **2015**, *23*, 2953−2974.
(39) Lo Fiego, M. J.; Lorenzetti, A. S.; Silbestri, G. F.; Domini, C. E. The use of ultrasound in the South Cone region. Advances in organic and inorganic synthesis and in analytical methods. *Ultrason. Sonochem.* **2021**, *80*, No. 105834.
(40) Thari, F. Z.; Tachallait, H.; El Alaoui, N-E.; Talha, A.; Arshad, S.; Álvarez, E.; Karrouchi, K.; Bougrin, K. Ultrasound-assisted one-pot green synthesis of new N- substituted-5-arylidene-thiazolidine-2,4-dione-isoxazoline derivatives using NaCl/Oxone/Na3PO4 in aqueous media. *Ultrason. Sonochem.* **2020**, *68*, No. 105222.
(41) Sharma, A.; Priya, A.; Kaur, M.; Singh, A.; Kaur, G.; Banerjee, B. Ultrasound-assisted synthesis of bioactive S-heterocycles. *Synth. Commun.* **2021**, *51*, 3209−3236.
(42) Marc, G.; Ionut, I.; Pirnau, A.; Vlase, L.; Vodnar, D. C.; Duma, M.; Tiperciuc, B.; Oniga, O. Microwave assisted synthesis of 3,5-disubstituted thiazolidine-2,4-diones with antifungal activity. Design, synthesis, virtual and in vitro antifungal screening. *Farmacia* **2017**, *65*, 414−422.
(43) Marc, G.; Stana, A.; Pirnau, A.; Vlase, L.; Vodnar, D. C.; Duma, M.; Tiperciuc, B.; Oniga, O. 3,5-Disubstituted thiazolidine-2,4-diones: Design, Microwave- Assisted synthesis, Antifungal activity and ADMET Screening. *SLAS Discovery* **2018**, *23*, 807−814.
(44) Nawale, S. L.; Avinash, S. D. Synthesis and evaluation of novel thiazolidinedione derivatives for antibacterial activity. *Der Pharma Chem.* **2012**, *4*, 2270−2277.
(45) C.C.G. Molecular Operating Environment (MOE), Montreal, Canada, 2014. http://www.chemcomp.com.
(46) Sala, F. A.; Wright, G. S. A.; Antonyuk, S. V.; Garratt, R. C.; Hasnain, S. S. Molecular recognition and maturation of SOD1 by its evolutionarily destabilized cognate chaperone hCCS. *PLoS Biol.* **2019**, *17*, No. e3000141.
(47) Daina, A.; Michielin, O.; Zoete, V. SwissADME: a free web tool to evaluate pharmacokinetics, drug-likeness and medicinal chemistry friendliness of small molecules. *Sci. Rep.* **2017**, *7*, No. 42717.
(48) Lipinski, C. A.; Lombardo, F.; Dominy, B. W.; Feeney, P. J. Experimental and computational approaches to estimate solubility and permeability in drug discovery and development settings. *Adv. Drug Delivery Rev.* **1997**, *23*, 3−25.
(49) Veber, D. F.; Johnson, S. R.; Cheng, H.-Y.; Smith, B. R.; Ward, K. W.; Kopple, K. D. Molecular Properties That Influence the Oral Bioavailability of Drug Candidates. *J. Med. Chem.* **2002**, *45*, 2615−2623.
(50) Muegge, I.; Heald, S. L.; Brittelli, D. Simple Selection Criteria for Drug-like Chemical Matter. *J. Med. Chem.* **2001**, *44*, 1841−1846.
(51) Ghose, A. K.; Viswanadhan, V. N.; Wendoloski, J. J. A knowledge-based approach in designing combinatorial or medicinal chemistry libraries for drug discovery. A qualitative and quantitative characterization of known drug databases. *J. Comb. Chem.* **1999**, *1*, 55−68.
(52) Banerjee, P.; Eckert, A. O.; Schrey, A. K.; Preissner, R. ProTox-II: a webserver for the prediction of toxicity of chemicals. *Nucleic Acids Res.* **2018**, *46*, 257−263.
(53) Kumar, D.; Narwal, S.; Sandhu, J. S. Catalyst-free synthesis of highly biologically active 5-arylidene rhodanine and 2,4-thiazolidine-dione derivatives using aldonitrones in polyethylene glycol. *Int. J. Med. Chem.* **2013**, *2013*, No. 273534.
(54) Da Silva, I. M.; Filho, J. S.; Santigo, P. B. G. S.; Do Egito, M. S.; De Souza, C. A.; Gouveia, F. L.; Ximenes, R. M.; Gouveia, K. X. F. L.; De Sena, K. X. F. R.; De Faria, A. R.; Brondani, D. J.; De Albuquerque, J. F. C. Synthesis and antimicrobial activities of 5-arylidene-thiazolidine-2,4-dione derivatives. *BioMed Res. Int.* **2014**, *2014*, No. 316082.
(55) Thirupathi, G.; Venkatanarayana, M.; Dubey, P. K.; Kumari, Y. B. Facile and green syntheses of substituted-5-arylidene-2,4-thiazolidinediones. *Der Pharma Chem.* **2012**, *4*, 2009−2013.
(56) Bhat, B. A.; Ponnala, S.; Sahu, D. P.; Tiwari, P.; Tripathi, B. K.; Srivastava, A. K. Synthesis and antihyperglycemic activity profiles of novel thiazolidinedione derivatives. *Bioorg. Med. Chem.* **2004**, *12*, 5857−5864.
(57) Graham, C. E.; Brocklehurst, K.; Pickergill, R. W.; Warren, M. J. Characterization of retinaldehyde dehydrogenase 3. *Biochem. J.* **2006**, *394*, 67−75.
(58) Rotruck, J. T.; Pope, A. L.; Ganther, H. E.; Swanson, A. B.; Hafeman, D. G.; Hoekstra, W. G. Selenium: biochemical role as a component of glutathione peroxidase. *Science* **1973**, *179*, 588−590.
(59) Marklund, S.; Marklund, G. Involvement of the superoxide anion radical in the autooxidation of pyrogallol and a convenient assay for superoxide dismutase. *Eur. J. Biochem.* **1974**, *47*, 469−474.

https://doi.org/10.1021/acsomega.2c02410
ACS Omega 2022, 7, 21267−21279